Revolutionizing Unmanned Aerial Vehicle Imagery Classification: A Deep Learning Approach Empowered by Computer Vision

Lee Xu

University of Chinese Academy of Sciences, CAS, Mathematics Department, Beijing, China

Leexu1244@yahoo.com

Abstract

Recently, computer vision, unmanned aerial vehicles (UAV) based remote sensing (RS) and deep learning (DL) technologies have been instrumental in global food productivity and future agriculture. UAV provides several advantages over other possible RS platforms like real-time data acquisition, high flexibility, and the best tradeoff between spatial, low cost, small size, spectral, and temporal resolution. One possible advantage of using UAVs for crop classification is that they can efficiently and quickly cover large areas, and could gather data from different angles and at different times. This might assist in providing detailed knowledge of the crops and their conditions. Earlier research is limited to finding a single crop from the RGB images taken by the UAV and hasn't explored the possibility of multi-crop classification by carrying out DL algorithms. Thus, this study presents a new Automated Crop Type Classification using Adaptive African Vulture Optimization with Deep Learning (ACCT-AAVODL) technique. The ACCT-AAVODL algorithm aims to investigate the UAV images and determine different types of food crops. To accomplish this, the presented ACCT-AAVODL method uses a densely connected network (DenseNet121) for generating feature vectors. Since the trial and error hyper parameter tuning is a challenging task, the AAVO model is employed for hyper parameter optimization. The ACCT-AAVODL technique involves a sparse auto encoder (SAE) with a Nadam optimizer for crop type classification, the stimulation analysis of the ACCT-AAVODL approach on the drone imagery dataset shows the remarkable performance of the ACCT-AAVODL method over other approaches.

Keywords: Unmanned aerial vehicles; Computer vision; Drone imagery; Agriculture; Food crop classification; Deep learning

1. Introduction

Agriculture is undoubtedly, one of the most prominent elements in economic development. It had an important role in structural transformation and long-term economic growth, though it might significantly differ by country [1]. Over the years, agricultural activities are commonly known for crop and food production. However, they have progressed in many nations to the marketing, distribution of crops, processing, and distribution of livestock products [2]. Nowadays, agriculture is formed as the primary source of livelihood, increases gross domestic product (GDP), a source of national trade, reduces unemployment, provides raw materials for manufacturing purposes, and overall develops the economy [3]. Recently, remote sensing (RS) with unmanned aerial vehicles (UAVs) has made perpetual progress in accurate agriculture, though UAVs were used for surveys, military, and other applications for a longer period [4]. Simply UAV is a type of unmanned system that includes camera sensors for capturing data with automated or manual flight management. It was widely inspected in precision agriculture since it has overcome many limitations that arise with satellite-based RS [5]. For example, firstly, it is flexible enough to revisit the field since the user can take it into flight at any time until there are any climatic changes. Then, it could capture high spatial resolution images very close to the plant [6]. Thirdly, it is easy to operate and deploy and also cost-effective. Lastly, it evades clouds by flying at lower heights and results in higher-quality images.

DOI: https://doi.org/10.54216/IJAACI.060205
Received: November 18, 2023 Revised: February 6, 2024 Accepted: July 4, 2024

UAVs otherwise called drones have a more flexible spectral and spatial resolution than the other RS platforms [7]. Also, land cover classification depends on RS image (RSI) was utilized in biodiversity conservation, agricultural management, urban planning, green vegetation classification, and land use. One important application of land cover classification was vegetation detection. Timely and Accurate data regarding the crop was a vital factor in enhancing crop production, which can be done through potential RS technologies [8]. Additionally, powerful techniques were decisive in using RS data efficiently. In modern agriculture, one fundamental key is crop classification, which classifies crop and plant types into different categories while describing their spatial distribution [9]. It could aid agriculturalists in having effectual data regarding their crops used for optimizing the making decision process. Several types of research were performed on accurate crop classification from satellite-based RSI through different deep learning (DL) and machine learning (ML) algorithms achieving extraordinary outcomes [10].

This study developed Automated Crop Type Classification using the Adaptive African Vulture Optimization with Deep Learning (ACCT-AAVODL) method. The presented ACCT-AAVODL method mainly employs a densely connected network (DenseNet121) for feature extractor with the AAVO technique as a hyper parameter optimizer. For crop type classification, the ACCT-AAVODL technique involves a sparse auto encoder (SAE) with a Nadam optimizer. The performance evaluation of the ACCT-AAVODL approach was performed on drone imagery datasets and the results are studied under various measures.

2. Related Works

Shi et al. [11] examine an end-to-end DL technique (CropdocNet) for correct and automated late blight disease analysis in UAV-based hyperspectral image (HIS). Based on the structural diversity of the canopy, the presented technique assumes the disease-specific reflectance radiation discrepancy and presents the objective class for representing the rotation invariance of objective classes from the feature spaces and several capsule layers for modelling the connection between spectral–spatial features. Li et al. [12] presented a novel technique for estimating fractional vegetation cover (FVC) such as half-Gaussian fitting for FVC (HAGFVC) and decomposing the Gaussian mixture method. During this technique, the histogram of the pure background pixel and pure vegetation pixel can initially properly utilize 2 half-Gaussian dispersions from the Commission International d'Eclairage (CIE) L*a*b* color space. Afterward, the threshold value was defined as dependent upon parameters of Gaussian distributions for generating a more exact FVC estimation. The authors developed low-altitude RS (LARS) imagery from 3 vegetative development steps at distinct flight altitudes on a cornfield.

In [13], an ensemble system was examined utilizing 2 distinct deep convolutional neural networks (DCNN) such as Multi-Filter Multiscale DCNN (MFMS-DCNN) and pre-training InceptionV3 structure, for crop classifier employing aerial image. Initially, the MFMS-DCNN was created utilizing a Convolutional-batch normalized-activation unit together with average and max pooling layers. At this point, an input image has been down sampled utilizing the max-pooling function rather than typical image processing systems that enable extracting the essential features from many levels, and the feature mapping can be integrated by embedding a step-wise fusion system. Chen et al. [14] propose a novel approach for crop row recognition in orthomosaic UAV images. Based on the statistics, a new crop detection technique using least square fitting was introduced and associated with the Hough transform-based technique for image preprocessing.

Wan et al. [15] introduce an ensemble modeling technique to phenotype crop FVC from UAV-based multi-spectral imagery by combining PROSAIL with gap probability models (PROSAIL-GP). The canopy image was attained by a UAV equipped with RGB and a multi-spectral camera. The author in [16], investigates the grey-level co-occurrence matrix (GLCM)-based text data for the crop classification with time-series UAV images and ML classifiers. Zhao et al. [17] proposed a fast mosaicking technique based on scale-invariant feature transform (SIFT) for mosaicking UAV images to monitor the growth of crop production. In the meantime, the random sample consensus (RANSAC) technique is incorporated for eliminating the effect of mismatched pairs in UAV imagery, the relative location relationship of UAV image takes place for monitoring the growth of the crop production and to retain the quality and accuracy of mosaicking.

3. Materials and Methods

In this study, a new ACCT-AAVODL approach was introduced for crop-type classification on UAV images. The presented ACCT-AAVODL technique follows a series of operations: DenseNet-121 feature extractor, AAVO-based hyper parameter optimizer, SAE classification, and Nadam hyper parameter tuning. The design of the AAVO algorithm helps to properly elect the hyper parameter values resulting in improved classification performance of the DenseNet-121 model. Fig. 1 demonstrates the working flow of the ACCT-AAVODL algorithm.

DOI: https://doi.org/10.54216/IJAACI.060205
Received: November 18, 2023 Revised: February 6, 2024 Accepted: July 4, 2024

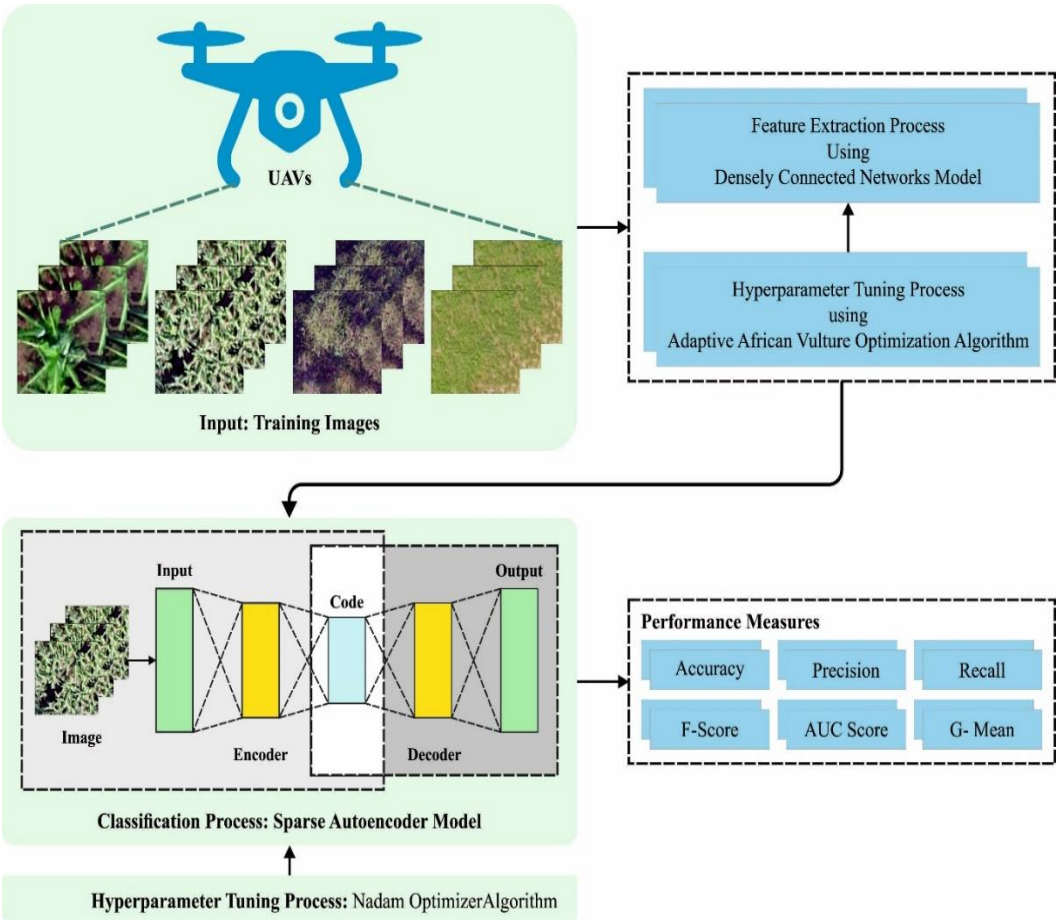

Fig 1. Workflow of ACCT-AAVODL approach

3.1. Data Used

The crop type classification outcomes of the ACCT-AAVODL system were tested utilizing the drone image dataset involving 6450 instances with six classes as represented in Table 1. RTI International (RTI) produced 2,611 labelled point locations demonstrating nineteen dissimilar land cover types, clustered in 5 different agro-ecological areas within Rwanda. This land cover type was minimized to three crop types (Legume, Maize, and Banana), two other non-cropland cover types (Structure and Forest), and catch-all other land cover types to provide evaluation training or data for the crop classification method. Every point is attributed to the land cover type, the degree of confidence, and latitude and longitude, the labeler had while categorizing the point location.

Table 1: Details of the dataset

Class Label	**Number of Sample Images**
Maize	2075
Banana	1661
Forest	1270
Other	750
Legume	363
Structure	331
Total No. of Sample Images	**6450**

DOI: https://doi.org/10.54216/IJAACI.060205
Received: November 18, 2023 Revised: February 6, 2024 Accepted: July 4, 2024

3.2. Feature Extraction: DenseNet-121 Model

The ACCT-AAVODL technique utilizes the DenseNet121 model for deriving the feature vector. For the deep architecture, the data path from input to output along with the gradient which travels the reverse way is so long that, some data are derived from the input layer until the output layer becomes larger, that they might get lost before they reach the destination [18]. Fig. 2 illustrates the architecture of DenseNet-121. This model modifies the connections among the layers stimulated by other network models, like, Fractal networks, Highway networks, and so on. In DenseNet, each layer is directly connected and utilizes the feature reusing concept that assists in reducing the overall amount of parameters. Another problem in the deep neural network (DNN) model that takes place during training is as follows the data flow and gradients. To resolve these issues, DenseNet provides the opportunity for each layer to directly access the gradient by comparing the loss function. Conventional feedforward Network bridges the outcomes of the layer to the immediate layer by implementing certain operations.

$$L_i = H_i(L_{i-1}) \tag{1}$$

In ResNet, Eq. (1) is adapted as Eq. (2).

$$L_i = H_i(L_{i-1}) + (L_{i-1}) \tag{2}$$

Rather than adding the outcome feature map of each block, it concatenates the maps as follows:

$$L_i = H_i([L_0, L_1, L_2, \dots \dots, L_{i-1}]) \tag{3}$$

Since the concatenation of each feature map could not be done simultaneously due to the size variance, DenseNet is divided into various blocks (DenseBlock). In all the blocks, the dimension of the map is considered a constant while, the filter number changes continuously. Transition Layers (TL) that assist in down-sample BN, a 1x1 convolution and 2x2 pooling layers. The DenseNet-121 model has been implemented in this study.

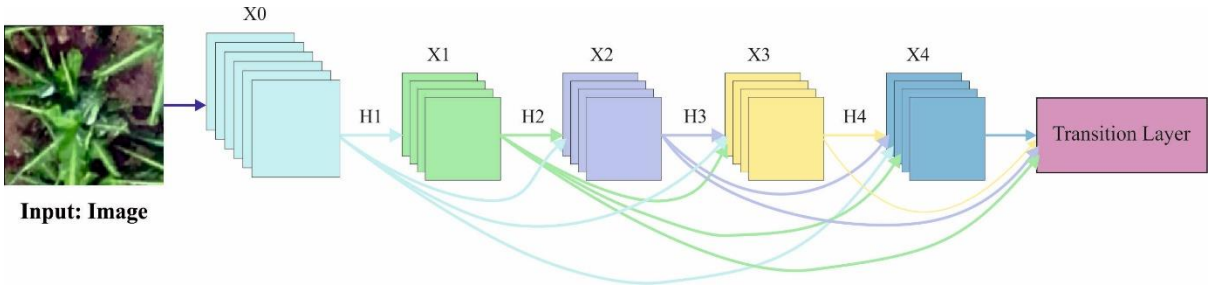

Fig 2. Structure of DenseNet-121 model

3.3. Hyper parameter Tuning: AAVO Algorithm

The AAVO technique is used for the optimum tuning process. The AVO model is based on vultures' search for food and competition with each other [19]. They fertilize feeble animals Even though this creature was predatory. Individuals who are incapable of ripping the carcasses stay for the friend to feed and slash on the carcass, and the weak vulture attacks the leftovers once they are full. The AVO technique is initiated by the random individual and later defines the aptitude afterward exploring the cost value. The finest vultures from the 2 clusters are recognized and saved as follows:

$$R_i = \begin{cases} Best\ vulture\ 1, if\ p_i = L_1 \\ Best\ vulture\ 2, if\ p_i = L_2 \end{cases} \tag{4}$$

$$L_1 + L_2 = 1 \tag{5}$$

where L_1 and L_2 represent the parameters that range from zero to one and are achieved beforehand optimization. The Roulette wheel model takes place to select the better individual in all the groups as follows:

$$p_i = \frac{F_i}{\Sigma_{j=1}^{m} F_i} \tag{6}$$

DOI: https://doi.org/10.54216/IJAACI.060205
Received: November 18, 2023 Revised: February 6, 2024 Accepted: July 4, 2024

Where F indicates the vulture's level of contentment. Then, compute the starvation ratio for the vulture. The vulture soars upward to find food and once the individual loses energy, the nearby strong vulture will compete for the food that is given below:

$$t = k \times \left(sin^{w} \left(\frac{\pi}{2} \times \frac{it_i}{\max_{it}} \right) + cos \left(\frac{\pi}{2} \times \frac{it_i}{\max_{it}} \right) - 1 \right) \quad (7)$$

$$F = (2 \times \delta_1 + 1) \times y \times \left(1 - \frac{it_i}{\max_{it}} \right) + t \quad (8)$$

Where it_i portray the existing iteration, w signifies the constant value to determine the optimization technique, δ_1 represents an arbitrary value in the limit [0,1], $\max_{it}$ signifies the overall amount of iterations, y is a random integer within $[-1,1]$, and k refers to the random integer within $[-2,2]$. When $y < 0$, then the vulture goes hungry; otherwise, it changes to one. Next, to achieve the exploration process, an arbitrary method with two approaches is developed:

If $P_1 < rand(P_1)$,

$$P(i+1) = R_i - F + \delta_2 \times \left((U - L) \times \delta_3 + lb \right) \quad (9)$$

If $P_1 > rand(P_1)$,

$$P(i+1) = R_i - D(i) \times F \quad (10)$$

where

$$D(i) = |X \times R(i) - P(i)| \quad (11)$$

Where R denotes better vulture, X signifies the randomly changing of vulture to save food taken from others using $X = 2 \times \delta_{i|i=1,2,3}$, L and U variables represent the lower and upper restrictions. Likewise, when $|H| < 1$, then the exploitation algorithm is implemented. The siege- and rotational flight indicated as P_2 and P_3 as 2 variables within [0,1]. The exploitation process begins if it ranges from 0.5 to 1. Vulture will be happy when $|H| \geq 1$. The frailer vulture seeks to attain food from the stronger one by using the following strategy:

$$P(i+1) = D(i) \times (F + \delta_4) - d(t) \quad (12)$$

$$d(t) = R_i - P(i) \quad (13)$$

Where δ_4 denotes the number within[0,1]. Furthermore, the vulture's spiral movement can be mathematically expressed as:

$$S_1 = R(i) \times \left(\frac{\delta_5 \times P(i)}{2\pi} \right) \times cos\left(P(i)\right) \quad (14)$$

$$S_2 = R(i) \times \left(\frac{\delta_6 \times P(i)}{2\pi} \right) \times sin\left(P(i)\right) \quad (15)$$

$$P(i+1) = R_j - (S_1 + S_2) \quad (16)$$

Where δ_5 and δ_6 indicate the random number ranges within [0,1]. When $|H| < 0.5$, the migration of vultures depends on hostile and siege fighting; they move to another site to acquire food. Mostly, the vulture will battle to gain food if δ_{P_3}, as a randomly generated number within [0,1], is equivalent to the P_3. Ig δ_{P_3} is lesser than P_3, then a violent siege-fight policy is applied. In a rare situation, vulture gets hungry, which leads to large rivalry amongst them to find food that is attained by the subsequent expression:

$$A_1 = BestVilture_1(i) - \frac{BestVilture_1(i) \times P(i)}{BestVilture_1(i) - P(i)^2} \times F \quad (17)$$

DOI: https://doi.org/10.54216/IJAACI.060205
Received: November 18, 2023 Revised: February 6, 2024 Accepted: July 4, 2024

$$A_2 = BestVilture_2(i) - \frac{BestVilture_2(i) \times P(i)}{BestVilture_2(i) - P(i)^2} \times F \quad (18)$$

Now $BestVilture(i)$ and $BestVilture(i)$ are the set of two best vultures, and $P(i)$ signifies the present vector location that can be obtained as follows:

$$P(i+1) = 0.5 \times (A_1 + A_2) \quad (19)$$

When $|F|$ is lesser than 0.5, then the previous healthy vulture loses energy and capability to fight against each other. Then, fly towards an unknown position to attain food:

$$P(i+1) = R(i) - |d(t)| \times F \times LF(d) \quad (20)$$

Where LP (Levy flight) can be attained by:

$$LF(x) = \frac{u \times \sigma}{100 \times |v|^2} \quad (21)$$

$$\sigma = \left(\frac{\Gamma(1+\rho) \times \sin\left(\frac{\pi\rho}{2}\right)}{\Gamma(1+\rho_2) \times \rho \times 2\left(\frac{\rho-1}{2}\right)}\right)^{\frac{1}{\rho}} \quad (22)$$

Where u and v are the random integers within $[0,1]$, and ρ defines the determined integer.

As mentioned earlier, the AVO is a new, efficient, biologically inspired algorithm for resolving optimization problems. The solution candidate has a randomly distributed value in the search range. A random walking strategy was utilized based on adaptive mechanisms, once the candidate has no neighbors, and the aforesaid method reduces the algorithm correctness and convergence trend. Thus, to tackle this problem, the adaptive learning factor (ALF) is needed. This can be achieved in the AAVO algorithm as shown below:

$$v = \frac{|f(P_i^j) - f(P_g^j)|}{f(P_g^j) + \varepsilon} \quad (23)$$

In Eq. (23), ε denotes the minimal constant to prevent zero-division-error, $f(P_i^i)$ and $f(P_g^j)$ show the i^{th} vulture's cost and ideal cost amount value at j^{th} iteration as follows:

$$d_i^t = \frac{1}{1 + e^{-g}} \quad (24)$$

Where g denotes the range within [0, 2]. Subsequently, the new satisfaction ratio was upgraded as follows:

$$F = (2 \times d_i^t + 1) \times y \times \left(1 - \frac{it_i}{\max_{it}}\right) + t \quad (25)$$

The AAVO algorithm derives a fitness function (FF) to get a better outcome of classification. It determines a positive integer to illustrate the greater efficacy of the solution candidate. The lessening classifying error rate is considered as an FF.

$$fitness(x_i) = ClassifierErrorRate(x_i)$$
$$= \frac{No.of\ misclassified\ instances}{Total\ no.of\ instances} * 100 \quad (26)$$

3.4. Crop Type Classification: Optimal SAE

In this study, the SAE algorithm is used for the classification of crop types on UAV images. Auto encoder (AE) is an unsupervised pretraining model that includes input, hidden, and decoding layers [20]. Auto encoder learns a characteristic transformation $h = f(Wx + b)$ by constructing three-layer networks of x to h to x. Especially, it makes it promising to employ sparsity constraint to the hidden unit to generate a variant of AE, viz., sparse AE

DOI: https://doi.org/10.54216/IJAACI.060205
Received: November 18, 2023 Revised: February 6, 2024 Accepted: July 4, 2024

(SAE). SAE learns features automatically from the unlabelled dataset, which provides better feature descriptions than the original dataset. In specific applications, if the feature found by SAE could replace the original dataset, they might lead to the best possible result. The SAE steps are given in the following:

Step1: Determine M number of hidden layers (HLs) and the connection weight between the input data and HLs, $w_i = [w_{1i}, w_{2i}, \dots w_{mi}]^T$, $(i = 1,2, \dots M)$ and the threshold value of the HLs, $b = [b_1, b_2, \dots, b_M]^T$. Later applying the original input x_k for training, the SAE could learn the h_k feature representations of the original input.

Step 2: Determine $a_j^{(2)}(x)$ as an activation value of j^{th} elements in the HL once a specific input x is given. The output of the sigmoid function value ranges in [0,1], 0 shows the suppression, and 1 denotes the activation. 0The constraint $\hat{\rho} = \rho$ is given below.

$$\hat{\rho} = \frac{1}{N}\sum_{i=1}^{N}[\, a_j^{(2)}(x^{(i)})] = \rho \tag{27}$$

Where ρ denotes the sparsity parameter that is usually a number closer to zero; N indicates the number of neurons.

Step 3: The study added Kullback-Leibler (KL) divergence as a penalty term to the loss function which controls the whole network for learning the expression of sparse features. The characteristics of KL divergence is that the nearer $\hat{p}$ gets to ρ, the smaller KL is, utilized for punishing $\hat{\rho}_j$ that deviates too much and makes $\hat{\rho}_j$ close to ρ in the training process.

$$\sum_{=1}^{M} K\, L(\rho \| \hat{\rho}_{\mathrm{j}}) = \sum_{j=1}^{M} \rho\, log\, \frac{\rho}{\hat{\rho}_j} + (1-\rho) log\, \frac{1-\rho}{1-\hat{\rho}_j} \tag{28}$$

Hence the loss function of SAE is:

$$J_{sparse}(W,b) = J(W,b) + \beta \sum_{j=1}^{M} K\, L(\rho \| \hat{\rho}_{\mathrm{j}}) \tag{29}$$

Here, W and b are the weight connecting and bias from the input to HLs correspondingly; $J(W,b)$ denotes a 1/2 square error cost function; M denotes the number of neurons in the HL. β used to weight control the sparse penalty term. The training aims for minimizing the target loss function $J_{sparse}(W,b)$. The partial derivative of the loss function is evaluated by (30) afterward adding KL divergence, where δ denotes the error term.

$$\delta_i^{(2)} = (\sum_{\mathrm{j}=1}^{M} W_{\mathrm{ji}}^{(3)}\, \delta_j^{(.3)}))f'(z_i^{(2)}) + \beta(-\frac{\rho}{\hat{p}_j} + \frac{1-\rho}{1-\hat{p}_j}) \tag{30}$$

Step 4: Afterward having a new partial derivative, backpropagation is adopted for optimizing the parameter of the whole network.

$$w_{ij}^{(2)} = W_{ij}^{(2)} - \alpha \frac{\partial}{\partial W_{ij}^{(2)}} J_{Sparse}(W,b) = W_{ij}^{(2)} - \alpha a_j^{(2)} \delta_j^{(3)} \tag{31}$$

$$b_i^{(2)} = b_i^{(2)} - \alpha \frac{\partial}{\partial b_i^{(2)}} J_{Sparse}(w,b) = b_i^{(2)} - \alpha \delta_j^{(3)} \tag{32}$$

From the above equations, α denotes the learning rate, W_{ij} signifies the weight connecting between i^{th} neurons of the input layer and j^{th} neurons of HL, and b_i signifies the bias. Next, the prediction method can be established afterward by iterative pre-training and normalizing the initial data by the SAE.

The Nadam optimizer is used for the training process to optimize the efficiency of the SAE model. The Nadam optimizer includes the incorporation of Nesterov momentum into the Adam optimizer (AO) [21]. The Nadam optimizer is discussed in detail. The weights are updated according to the recursive law. In contrast to AO, the

DOI: https://doi.org/10.54216/IJAACI.060205
Received: November 18, 2023 Revised: February 6, 2024 Accepted: July 4, 2024

Nadam optimizer converges fast and is better suited for the pretraining phase. The exponential decay rate β_1 and β_2, the fuzz factor τ, the time step k, and the learning rate η_1 the first- and the second-order estimate mk and n_k, are the initialized parameters and it can be formulated as follows:

$$\beta_1^k = \beta_1\left(1 - 0.5 \times 0.96^{\frac{k}{250}}\right) \tag{33}$$

Where $\beta_1 = 0.99$. the iterative method plays a major part in this algorithm. The initial stage is to evaluate the gradient loss function (w_{k-1}^s), and w_{k-1}^s denotes the weight parameter. Next, evaluate the estimate m_k and n_k at $the\ k^{th}$ time step. $\hat{m}k$ and $\hat{n}k$ unbiased estimations are obtained after correction. The latter step is to upgrade the weight parameter. Next, the procedure is reiterated until the optimal value is reached.

4. Performance Validation

In this section, the crop type classification outputs of the ACCT-AAVODL technique are investigated by the drone image dataset including 6450 samples with six classes. The confusion matrices of the ACCT-AAVODL technique under the crop type classification procedure are portrayed in Fig. 3. The result indicates that the ACCT-AAVODL method recognizes all the crops accurately. For instance, on 70% of TRAS, the ACCT-AAVODL method categorizes 1370 samples into maize, 1149 samples into a banana, 812 samples into the forest, 495 samples into others, 215 samples into legume, and 181 samples into the structure. Meanwhile, on 80% of the TRAS, the ACCT-AAVODL method classifies 1603 samples into maize, 1297 samples into a banana, 975 samples into the forest, 549 samples into others, 248 samples into legume, and 240 samples into the structure.

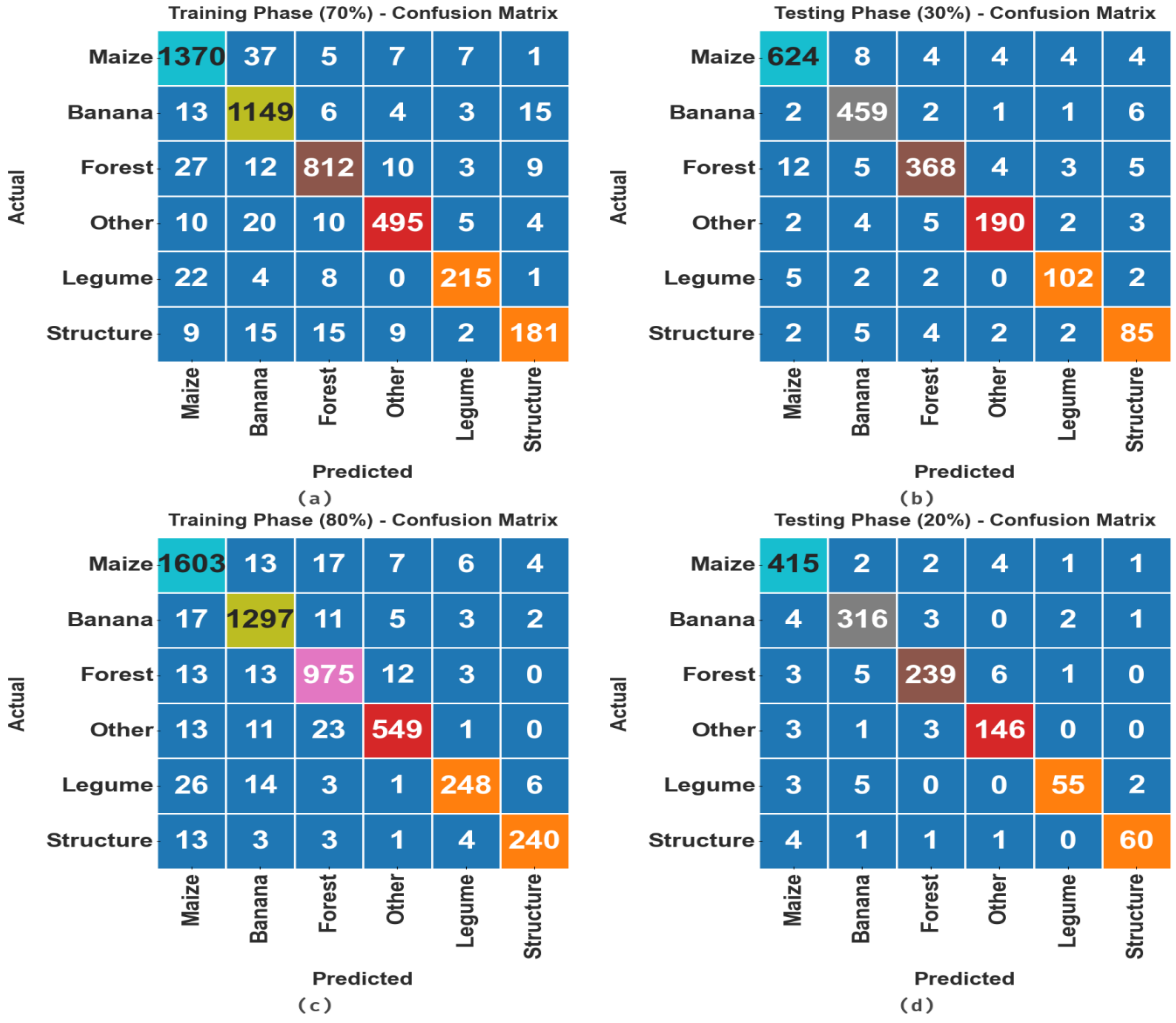

Fig 3. Confusion matrices of ACCT-AAVODL approach (a-b) TRAS/TESS of 70:30 and (c-d) TRAS/TESS of 80:20

DOI: https://doi.org/10.54216/IJAACI.060205
Received: November 18, 2023 Revised: February 6, 2024 Accepted: July 4, 2024

In Table 2, the overall crop type classification outputs of the ACCT-AAVODL method are investigated on 70:30 of the TR set (TRAS)/TS set (TESS). The outcomes ensured that the ACCT-AAVODL technique detected six classes proficiently. On 70% of the TRAS, the ACCT-AAVODL method achieves an average $accu_y$ of 97.84%, $prec_n$ of 92.29%, $reca_l$ of 90.15%, F_{score} of 91.16%, AUC_{score} of 94.38%, and G_{mean} of 94.21%. Simultaneously, on 30% of TESS, the ACCT-AAVODL algorithm achieves an average $accu_y$ of 98.16%, $prec_n$ of 92.00%, $reca_l$ of 92.32%, F_{score} of 92.15%, AUC_{score} of 95.59%, and G_{mean} of 95.50%.

Table 2: Crop type classifier outcome of ACCT-AAVODL method on 70:30 of TRAS/TESS

Class	Acc_y	$Prec_n$	$Reca_l$	F_{score}	AUC_{score}	G_{mean}
Training Phase (70%)						
Maize	96.94	94.42	96.01	95.21	96.69	96.69
Banana	97.14	92.89	96.55	94.68	96.95	96.95
Forest	97.67	94.86	93.01	93.93	95.90	95.86
Other	98.25	94.29	90.99	92.61	95.12	95.03
Legume	98.78	91.49	86.00	88.66	92.77	92.52
Structure	98.23	85.78	78.35	81.90	88.83	88.21
Average	**97.84**	**92.29**	**90.15**	**91.16**	**94.38**	**94.21**
Testing Phase (30%)						
Maize	97.57	96.45	96.30	96.37	97.25	97.25
Banana	98.14	95.03	97.45	96.23	97.91	97.91
Forest	97.62	95.58	92.70	94.12	95.79	95.74
Other	98.60	94.53	92.23	93.37	95.80	95.73
Legume	98.81	89.47	90.27	89.87	94.80	94.69
Structure	98.19	80.95	85.00	82.93	91.96	91.69
Average	**98.16**	**92.00**	**92.32**	**92.15**	**95.59**	**95.50**

Fig 4. TRAA and VAAC outcomes of ACCT-AAVODL method on 70:30 of TRAS/TESS

DOI: https://doi.org/10.54216/IJAACI.060205
Received: November 18, 2023 Revised: February 6, 2024 Accepted: July 4, 2024

The TRAA and VAAC of the ACCT-AAVODL approach on 70:30 of the TRAS/TESS is portrayed in Fig. 4. The figure indicated that the ACCT-AAVODL approach has shown better outcomes with increased values of TRAA and VAAC. The ACCT-AAVODL model has gained the highest TRAA outcome.

The TRALS and VALS of the ACCT-AAVODL model on 70:30 of the TRAS/TESS are portrayed in Fig.5. The figure denoted that the ACCT-AAVODL model has demonstrated superior outcome with the least values of TRALS and VALS. The ACCT-AAVODL technique has given an output in minimized VALS outputs.

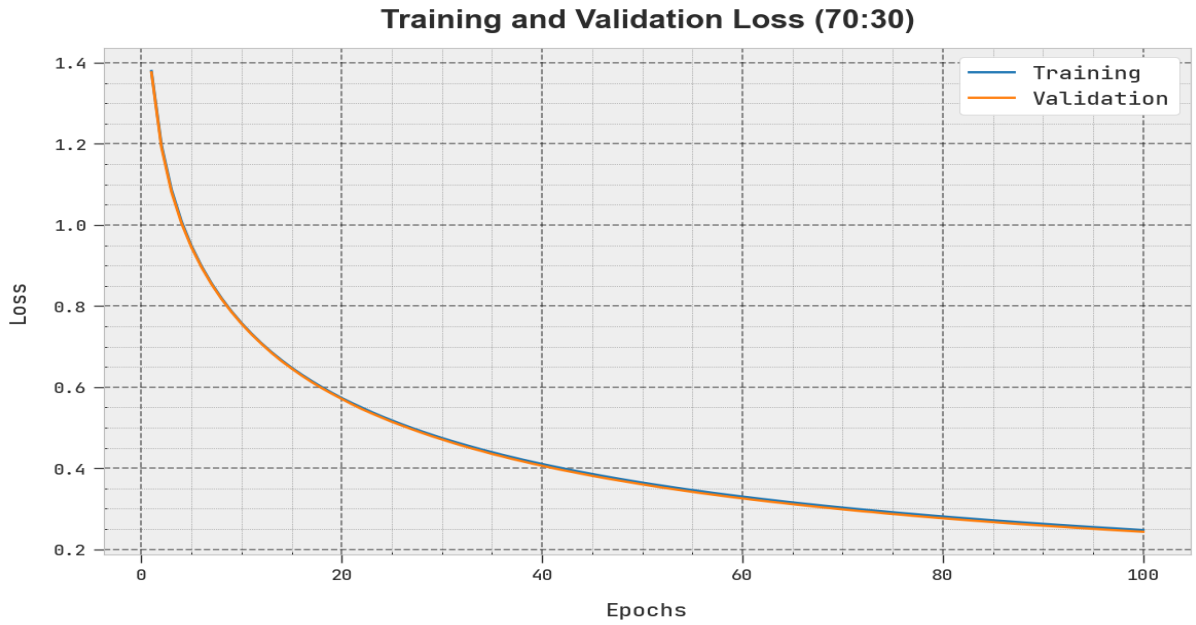

Fig 5. TRALS and VALS outcome of ACCT-AAVODL system on 70:30 of TRAS/TESS

In Table 3, the overall crop type classification output of the ACCT-AAVODL technique is investigated under 80:20 of the TRAS/TESS. The outcomes assured that the ACCT-AAVODL method recognized six classes. On 80% of the TRAS, the ACCT-AAVODL method achieves an average $accu_y$ of 98.40%, $prec_n$ of 94.99%, $reca_l$ of 92.73%, F_{score} of 93.79%, AUC_{score} of 95.84%, and G_{mean} of 95.75%. Simultaneously, on 20% of the TESS, the ACCT-AAVODL system achieves an average $accu_y$ of 98.48%, $prec_n$ of 94.69%, $reca_l$ of 93.04%, F_{score} of 93.82%, AUC_{score} of 96.03%, and G_{mean} of 95.95%.

Table 3: Crop type classifier outcome of ACCT-AAVODL model on 80:20 of TRAS/TESS

Class	Acc_y	$Prec_n$	$Reca_l$	F_{score}	AUC_{score}	G_{mean}
Training Phase (80%)						
Maize	97.50	95.13	97.15	96.13	97.41	97.41
Banana	98.22	96.00	97.15	96.57	97.87	97.87
Forest	98.10	94.48	95.96	95.21	97.29	97.29
Other	98.57	95.48	91.96	93.69	95.69	95.62
Legume	98.70	93.58	83.22	88.10	91.44	91.07
Structure	99.30	95.24	90.91	93.02	95.33	95.23
Average	**98.40**	**94.99**	**92.73**	**93.79**	**95.84**	**95.75**
Testing Phase (20%)						
Maize	97.91	96.06	97.65	96.85	97.84	97.84
Banana	98.14	95.76	96.93	96.34	97.74	97.74
Forest	98.14	96.37	94.09	95.22	96.61	96.58
Other	98.60	92.99	95.42	94.19	97.23	97.21
Legume	98.91	93.22	84.62	88.71	92.14	91.84
Structure	99.15	93.75	89.55	91.60	94.61	94.48
Average	**98.48**	**94.69**	**93.04**	**93.82**	**96.03**	**95.95**

DOI: https://doi.org/10.54216/IJAACI.060205
Received: November 18, 2023 Revised: February 6, 2024 Accepted: July 4, 2024

The TRAA and VAAC of the ACCT-AAVODL technique on 80:20 of the TRAS/TESS are described in Fig. 6. The figure indicated that the ACCT-AAVODL technique has exhibited better outcomes with the highest values of TRAA and VAAC. The ACCT-AAVODL method has achieved a high TRAA outcome.

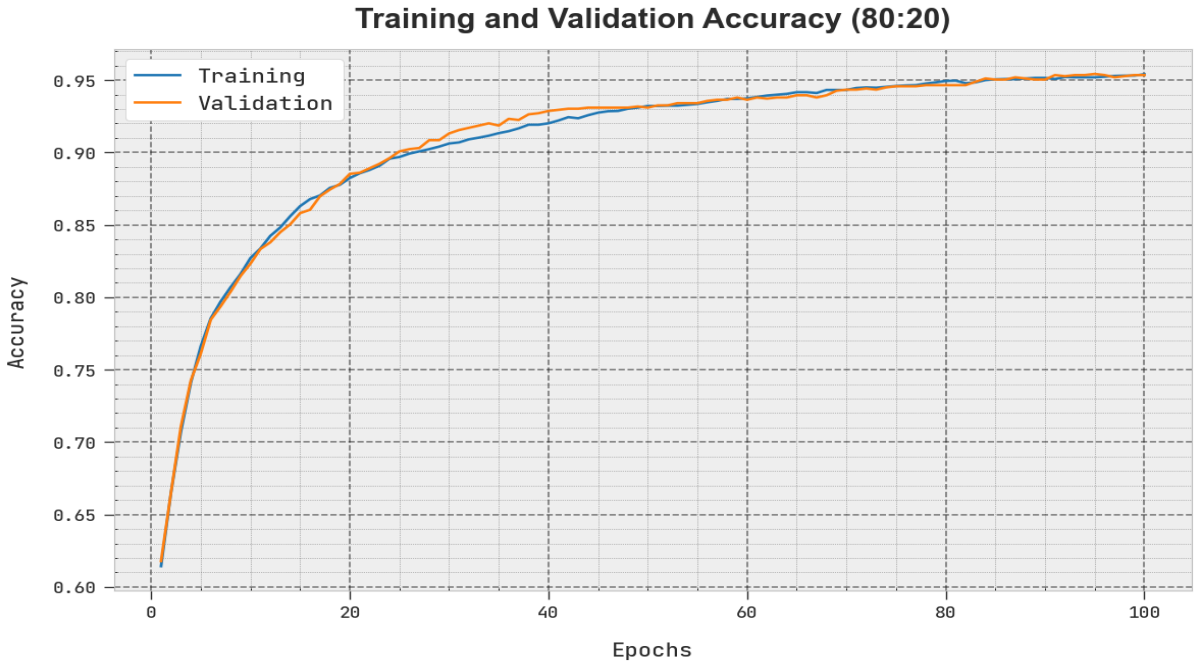

Fig 6. TRAA and VAAC outcomes of ACCT-AAVODL system on 80:20 of TRAS/TESS

The TRALS and VALS of the ACCT-AAVODL approach on 80:20 of the TRAS/TESS are shown in Fig. 7. The outcome reported that the ACCT-AAVODL approach has obtained greater achievement with the lowest values of TRALS and VALS. The ACCT-AAVODL method has resulted in minimized VALS outputs.

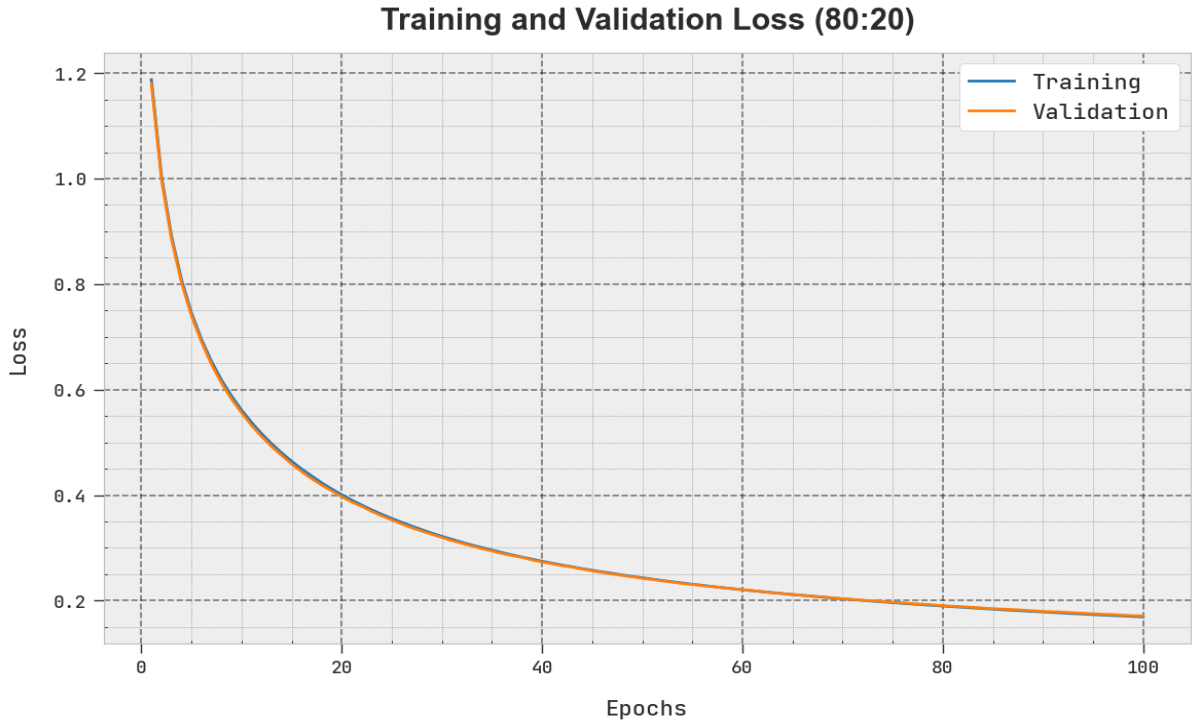

Fig 7. TRALS and VALS outcomes of ACCT-AAVODL system on 80:20 of TRAS/TESS

DOI: https://doi.org/10.54216/IJAACI.060205
Received: November 18, 2023 Revised: February 6, 2024 Accepted: July 4, 2024

The classifier results of the ACCT-AAVODL technique at 70:30 and 80:20 is demonstrated in Fig 8. Figs. The PR analysis of the ACCT-AAVODL technique is depicted in Figs. 8a-8c. The outputs reported that the ACCT-AAVODL technique has gained high PR performance in all classes. Finally, the ROC examination of the ACCT-AAVODL method is illustrated in Figs. 8b-8d. The figure indicated that the ACCT-AAVODL system has given an output in effective outputs with high ROC values on discrete classes.

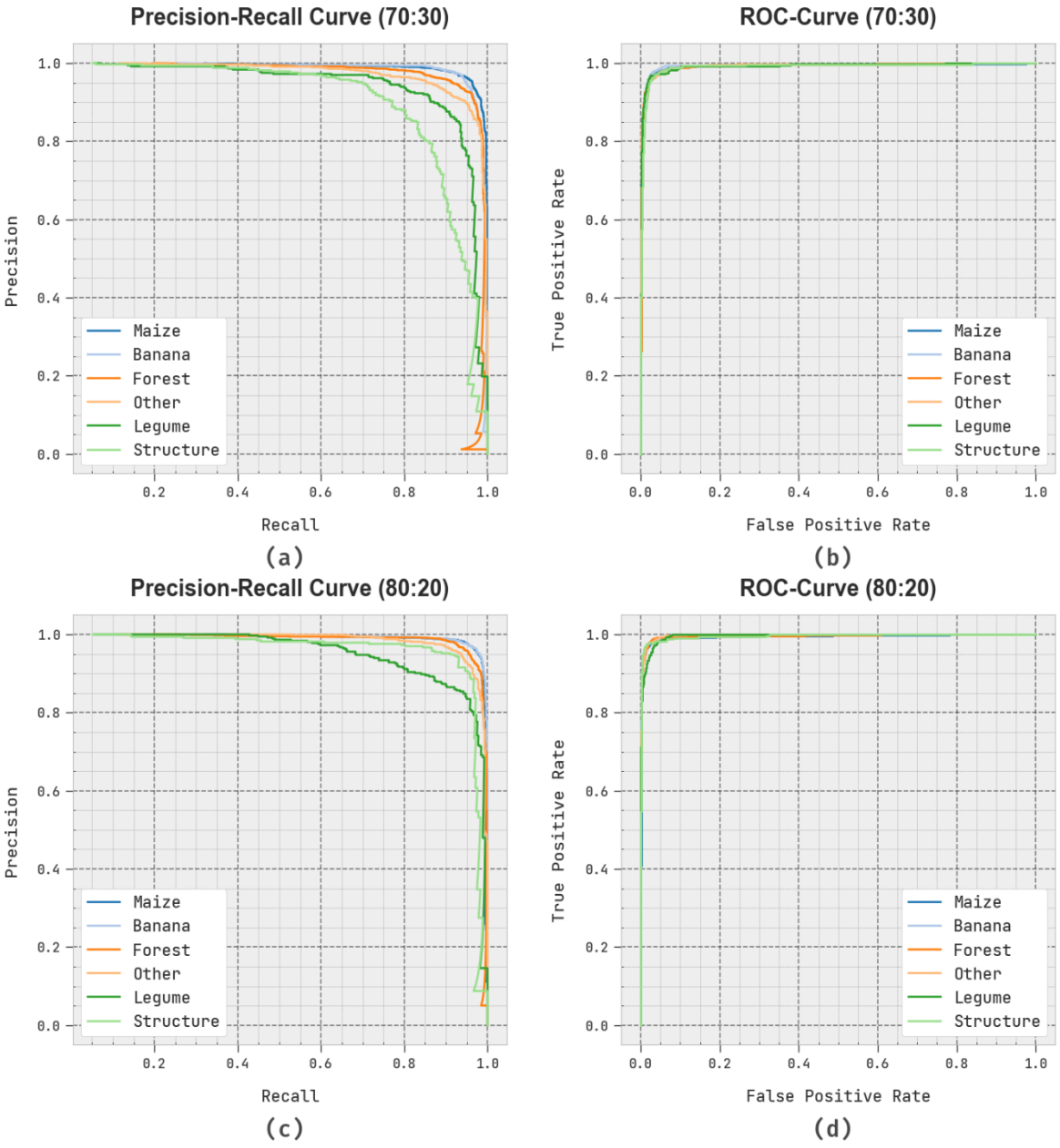

Fig. 8. 70:30 and 80:20 of (a-c) PR curve and (b-d) ROC curve

A detailed comparison analysis is performed in Table 4 to highlight the greater achievement of the ACCT-AAVODL technique. Fig. 9 examines comparative $accu_y$ outputs of the ACCT-AAVODL technique with existing approaches. The outputs indicate that the DNN-TL, ResNet, and SVM models accomplish the least $accu_y$ values of 87.36%, 87.39%, and 87.66% respectively. Moreover, the VGG-16 model reaches a slightly enhanced $accu_y$ of 89.98%. Although the AlexNet model resulted in near-optimal $accu_y$ of 91.68%, the ACCT-AAVODL technique obtains the highest $accu_y$ of 98.48%.

DOI: https://doi.org/10.54216/IJAACI.060205
Received: November 18, 2023 Revised: February 6, 2024 Accepted: July 4, 2024

Table 4: Comparative output of ACCT-AAVODL technique with current methods

Methods	Acc_y	$Prec_n$	$Reca_l$	F_{score}
ACCT-AAVODL	98.48	94.69	93.04	93.82
DNN-TL	87.36	87.11	85.50	86.44
AlexNet	91.68	87.80	82.21	84.32
VGG-16	89.98	84.98	81.32	86.26
ResNet	87.39	86.11	81.63	82.98
SVM	87.66	88.28	83.97	84.58

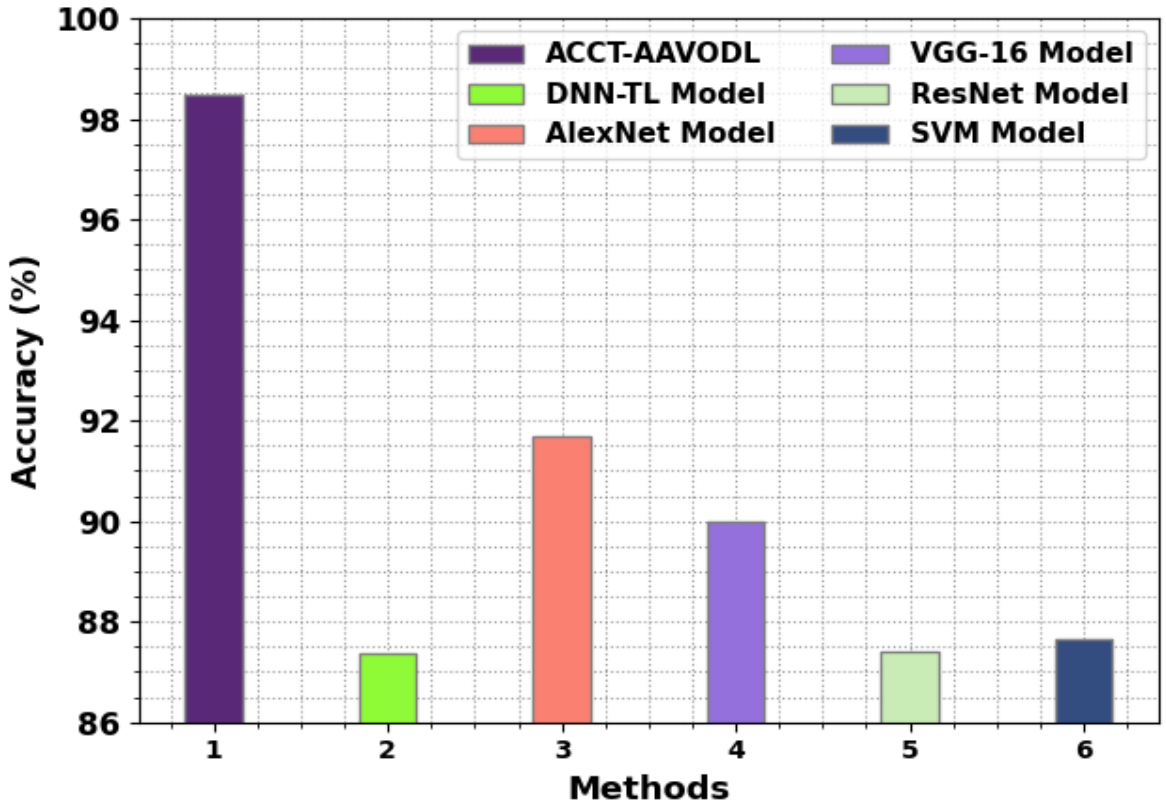

Fig 9. $Accu_y$ Outcome of ACCT-AAVODL technique with existing methods

Fig. 10 examines comparative $prec_n$ results of the ACCT-AAVODL method with present approaches. The result indicates that the VGG-16, ResNet, and DNN-TL models accomplish the least $prec_n$ values of 84.98%, 86.11%, and 87.11% correspondingly. Furthermore, the AlexNet model reaches a slightly enhanced $prec_n$ of 87.8%. Although the SVM approach results in a near-optimal $prec_n$ of 88.28%, the ACCT-AAVODL system attains the highest $prec_n$ of 94.69%.

Fig. 11 examines a relative $reca_l$ results of the ACCT-AAVODL model with present approaches. The result indicates that the VGG-16, ResNet, and AlexNet models accomplish the least $reca_l$ values of 81.32%, 81.63%, and 82.21% correspondingly. Furthermore, the SVM model reaches a slightly improved $reca_l$ of 83.97%. Although the DNN-TL method resulted in a near-optimal $reca_l$ of 85.5%, the ACCT-AAVODL technique obtained the highest $reca_l$ of 93.04%.

DOI: https://doi.org/10.54216/IJAACI.060205
Received: November 18, 2023 Revised: February 6, 2024 Accepted: July 4, 2024

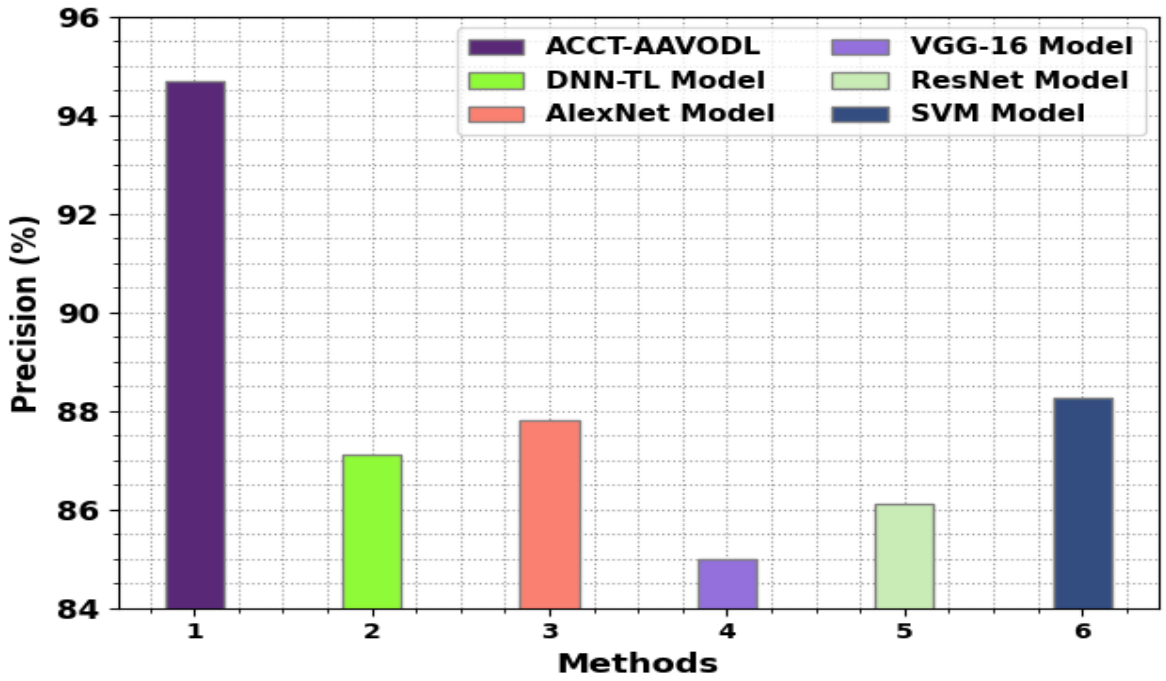

Fig 10. $Prec_n$ Outcome of ACCT-AAVODL technique with existing methods

Fig. 12 examines the comparative F_{score} results of the ACCT-AAVODL method with present approaches. The result indicates that the ResNet, AlexNet, and SVM methods accomplish the lowest F_{score} values of 82.98%, 84.32%, and 84.58% correspondingly.

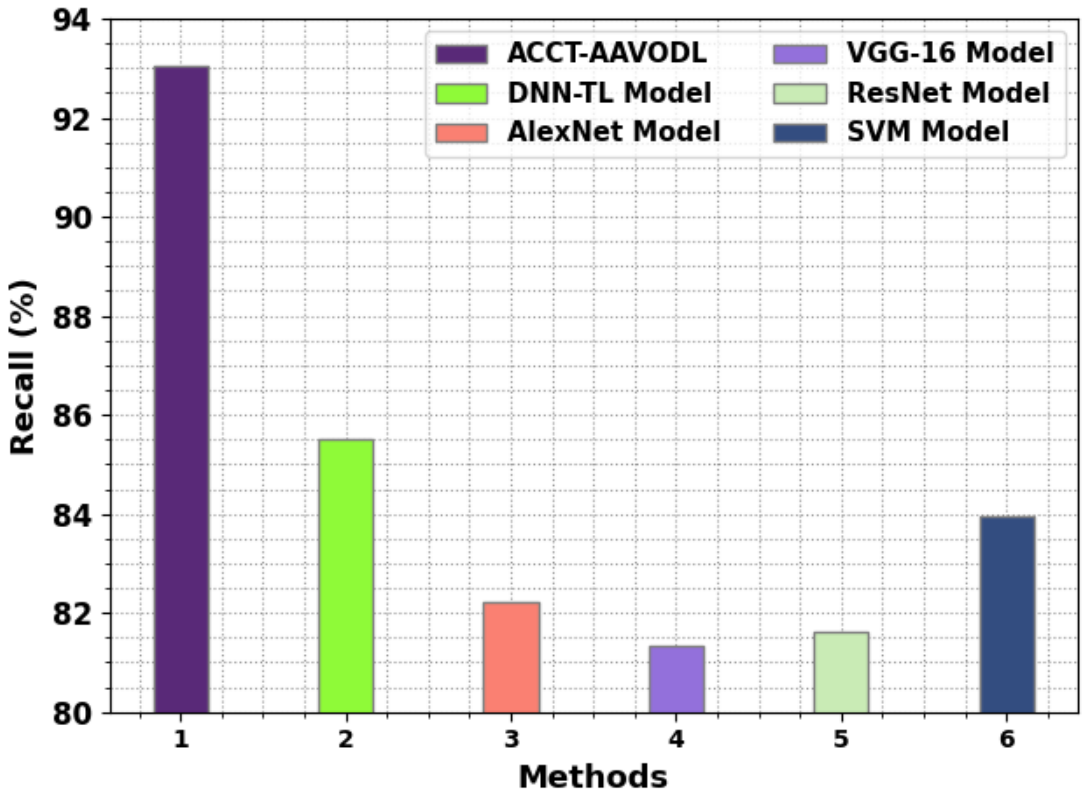

Fig 11. $Reca_l$ Outcome of ACCT-AAVODL system with existing algorithms

DOI: https://doi.org/10.54216/IJAACI.060205
Received: November 18, 2023 Revised: February 6, 2024 Accepted: July 4, 2024

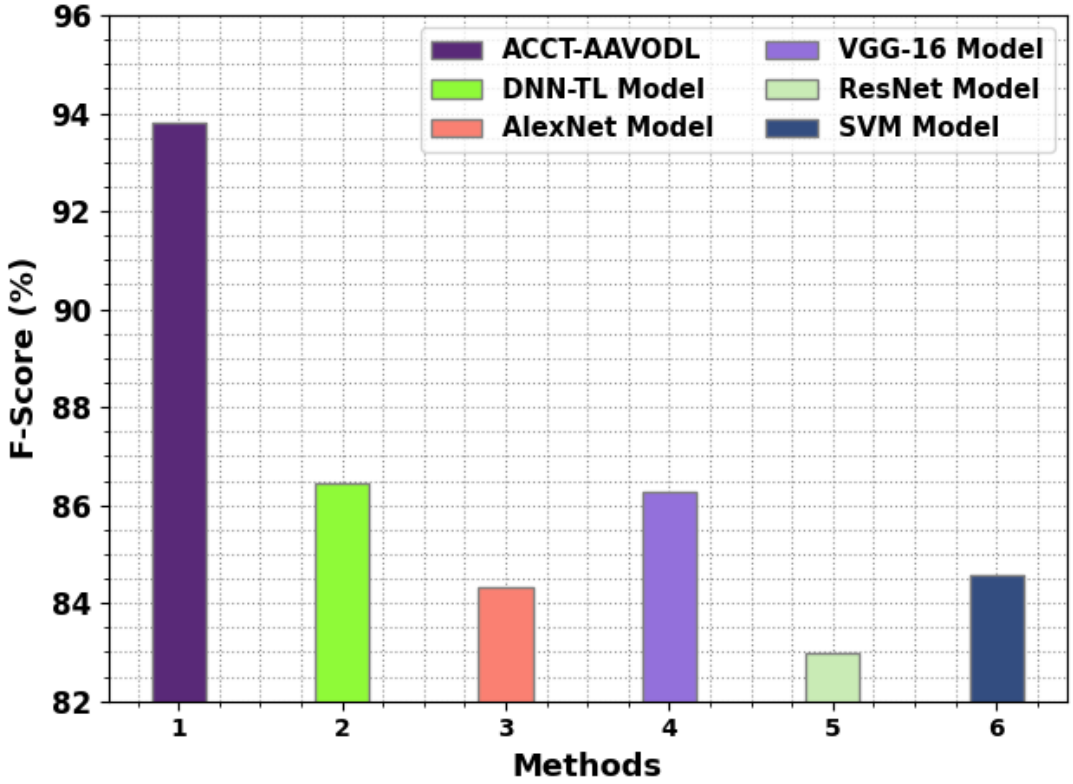

Fig 12. F_{score} Outcome of ACCT-AAVODL system with existing algorithms

Furthermore, the VGG-16 model reaches a slightly improved F_{score} of 86.26%. Although the DNN-TL method resulted in a near-optimal F_{score} of 86.44%, the ACCT-AAVODL method gained the highest F_{score} of 93.82%. This result ensured the greater efficiency of the ACCT-AAVODL technique over other DL models.

5. Conclusion

In this study, a new ACCT-AAVODL approach was introduced for crop-type classification on UAV images. The proposed ACCT-AAVODL method follows a series of operations: DenseNet-121 feature extractor, AAVO-based hyper parameter optimizer, SAE classification, and Nadam tuning. The design of the AAVO method helps to properly elect the hyper parameter values which leads to better classification accuracy of DenseNet-121 architecture. The performance evaluation of the ACCT-AAVODL algorithm takes place on a drone imagery dataset and the outcomes are studied under various measures. The investigational output analysis demonstrates the remarkable performance of the sACCT-AAVODL method over other techniques for crop type classification. In the future, advanced DL classification algorithms can be employed to optimize classification accuracy. In addition, the ACCT-AAVODL technique is tested under real-time large-scale datasets.

References

[1] Orynbaikyzy, A., Gessner, U. and Conrad, C., 2019. Crop type classification using a combination of optical and radar remote sensing data: A review. *International journal of remote sensing*, *40*(17), pp.6553-6595.

[2] Johnson, D.M. and Mueller, R., 2021. Pre-and within-season crop type classification trained with archival land cover information. *Remote Sensing of Environment*, *264*, p.112576.

[3] Heupel, K., Spengler, D. and Itzerott, S., 2018. A progressive crop-type classification using multitemporal remote sensing data and phenological information. *PFG–Journal of Photogrammetry, Remote Sensing and Geoinformation Science*, *86*(2), pp.53-69.

[4] Hao, P., Wu, M., Niu, Z., Wang, L. and Zhan, Y., 2018. Estimation of different data compositions for early-season crop type classification. *PeerJ*, *6*, p.e4834.

DOI: https://doi.org/10.54216/IJAACI.060205
Received: November 18, 2023 Revised: February 6, 2024 Accepted: July 4, 2024

[5] Nowakowski, A., Mrziglod, J., Spiller, D., Bonifacio, R., Ferrari, I., Mathieu, P.P., Garcia-Herranz, M. and Kim, D.H., 2021. Crop type mapping by using transfer learning. *International Journal of Applied Earth Observation and Geoinformation*, *98*, p.102313.

[6] Giordano, S., Bailly, S., Landrieu, L. and Chehata, N., 2020. Improved crop classification with rotation knowledge using sentinel-1 and-2 time series. *Photogrammetric Engineering & Remote Sensing*, *86*(7), pp.431-441.

[7] Feng, S., Zhao, J., Liu, T., Zhang, H., Zhang, Z. and Guo, X., 2019. Crop type identification and mapping using machine learning algorithms and sentinel-2 time series data. *IEEE Journal of Selected Topics in Applied Earth Observations and Remote Sensing*, *12*(9), pp.3295-3306.

[8] Tseng, G., Zvonkov, I., Nakalembe, C.L. and Kerner, H., 2021, August. CropHarvest: A global dataset for crop-type classification. In *the Thirty-fifth Conference on Neural Information Processing Systems Datasets and Benchmarks Track (Round 2)*.

[9] M Rustowicz, R., Cheong, R., Wang, L., Ermon, S., Burke, M. and Lobell, D., 2019. Semantic segmentation of crop type in Africa: A novel dataset and analysis of deep learning methods. In *Proceedings of the IEEE/CVF Conference on Computer Vision and Pattern Recognition Workshops* (pp. 75-82).

[10] Zhang, H., Kang, J., Xu, X., and Zhang, L., 2020. Accessing the temporal and spectral features in crop type mapping using multi-temporal Sentinel-2 imagery: A case study of Yi'an County, Heilongjiang province, China. *Computers and Electronics in Agriculture*, *176*, p.105618.

[11] Shi, Y., Han, L., Kleerekoper, A., Chang, S. and Hu, T., 2022. Novel CropdocNet Model for Automated Potato Late Blight Disease Detection from Unmanned Aerial Vehicle-Based Hyperspectral Imagery. *Remote Sensing*, *14*(02), p.396.

[12] Li, L., Mu, X., Macfarlane, C., Song, W., Chen, J., Yan, K. and Yan, G., 2018. A half-Gaussian fitting method for estimating fractional vegetation cover of corn crops using unmanned aerial vehicle images. *Agricultural and Forest Meteorology*, *262*, pp.379-390.

[13] Kalita, I., Singh, G.P. and Roy, M., 2022. Crop classification using aerial images by analyzing an ensemble of DCNNs under multi-filter & multi-scale framework. *Multimedia Tools and Applications*, pp.1-25.

[14] Chen, P., Ma, X., Wang, F. and Li, J., 2021. A New Method for Crop Row Detection Using Unmanned Aerial Vehicle Images. *Remote Sensing*, *13*(17), p.3526.

[15] Wan, L., Zhu, J., Du, X., Zhang, J., Han, X., Zhou, W., Li, X., Liu, J., Liang, F., He, Y. and Cen, H., 2021. A model for phenotyping crop fractional vegetation cover using imagery from unmanned aerial vehicles. *Journal of experimental botany*, *72*(13), pp.4691-4707.

[16] Kwak, G.H. and Park, N.W., 2019. Impact of texture information on crop classification with machine learning and UAV images. *Applied Sciences*, *9*(4), p.643.

[17] Zhao, J., Zhang, X., Gao, C., Qiu, X., Tian, Y., Zhu, Y. and Cao, W., 2019. Rapid mosaicking of unmanned aerial vehicle (UAV) images for crop growth monitoring using the SIFT algorithm. *Remote Sensing*, *11*(10), p.1226.

[18] Charchekhandra, B. (2023). Align and fusion two thermal and visual images. *Pure Mathematics for Theoretical Computer Science*, 1(1), 17-31.

[19] Hazarika, R.A., Kandar, D. and Maji, A.K., 2022. An experimental analysis of different deep learning-based models for Alzheimer's disease classification using brain magnetic resonance images. *Journal of King Saud University-Computer and Information Sciences*, *34*(10), pp.8576-8598.

[20] Baghbadorani, S.B., Johari, S.A., Fakhri, Z., Shahmirzadi, E.K., Shavkatovich, S.N. and Lee, S., 2022. A New Version of African Vulture Optimizer for Apparel Supply Chain Management Based on Reorder Decision-Making. *Sustainability*, *15*(1), pp.1-18.

[21] Li, Z., Peng, F., Niu, B., Li, G., Wu, J. and Miao, Z., 2018. Water quality prediction model combining sparse auto-encoder and LSTM network. *IFAC-PapersOnLine*, *51*(17), pp.831-836.

[22] Koushik, S.S. and Srinivasa, K.G., 2021. Detection of respiratory diseases from chest X-rays using Nesterov accelerated adaptive moment estimation. *Measurement*, *176*, p.109153.

DOI: https://doi.org/10.54216/IJAACI.060205
Received: November 18, 2023 Revised: February 6, 2024 Accepted: July 4, 2024